Visible photon avalanche up-conversion of Yb^{3+} and Ho^{3+} doped $NaBi(WO_4)_2$ phosphors under excitation at 980 nm

Haiyue Qian[1,*] , Tianqing Zhang[2], Xiliang Jiang[2], Haihao Wang[1], Weiling Yang[2], and Chun Li[2,*]

[1] *JiLin Technology College of Electronic Information, JiLin 132021, China*
[2] *School of Materials Science and Engineering, Changchun University of Science and Technology, Changchun 130022, China*

ABSTRACT

Avalanche phenomenon uses critical pump power to produce extreme nonlinear behavior from small disturbances, and has gradually become known. Here, it is reported that the strong green up-conversion emission produced in NaBi $(WO_4)_2$ phosphor by the positive feedback enhancement of the energy transfer process. The power dependence indicates that the photon avalanche process has occurred. Contrary to other up-conversion mechanisms, photon avalanche (PA) is a bifurcation phenomenon: avalanches occur above the critical excitation power. The experimental results are analyzed using the rate equation model. The high-response photon avalanche process produced by Yb and Ho ions is discussed in detail. The results show that PA can not only improve the brightness and efficiency of up-conversion, but also has a wider range of applications than traditional up-conversion materials, especially in the detection material of temperature sensor plays an important role.

1 Introduction

In recent years, rare earth (RE)-doped luminescent materials have attracted more and more attention. The electric dipole transition and the magnetic dipole transition cause the photoluminescence of RE ions. In addition, one of the most valuable properties of these materials is "up-conversion (UC)," which converts low-energy photons (infrared or visible light) into high-energy photons through the process of multi-photon absorption or energy transfer, this makes UC

phosphors widely used in optical temperature sensors and photoelectric sensor. Traditional sensors rely on the expansion principle of liquids and metals, or have low infrared conversion efficiency. Therefore, they cannot be used in harsh environments, and the sensing accuracy is low, which makes them no longer meet the needs of current social sciences, the UC fluorescence intensity ratio (FIR) technique is considered to be one of the state-of-the-art [1–9]. UC luminescence occurs through three mechanisms: (1) ground state absorption (GSA); (2) excited state

Address correspondence to E-mail: q270305368@126.com; lichun1210@163.com

absorption (ESA) and continuous energy transfer (ETU) from donor to up-conversion acceptor; (3) and photon avalanche. Among them, the PA process is relatively rare and is one of the most effective UC processes. In the PA process, when the pump power reaches the threshold, the number of excited particles rises sharply due to the cross-relaxation, resulting in strong up-conversion emission, due to these special characteristics, these materials have huge applications in various fields such as optical temperature measurement, laser devices, display devices, optical amplifiers, fingerprint printing, and biological imaging [10–21].

The biggest advantage of the PA process is that it not only has an extreme nonlinear effect but also a high efficiency, and there is no periodic photon emission or interference effect. The PA phenomenon was discovered for the first time in Pr^{3+} ion-doped crystals. It was found that when the excitation exceeds the critical pump laser intensity, the up-conversion luminescence suddenly increases. This special property quickly promoted development of other PA materials, such as high-efficiency up-conversion lasers. The PA phenomenon is mainly observed at low temperatures, with some exceptions at room temperature. Lahoz reported a very strong green band at room temperature in Ho^{3+}-doped fluoroindium glass under excitation at 747 nm. Temporal dynamics based on strong excited state absorption and processes suggest that a photon avalanche mechanism occurs. Auzel F reported the photonic avalanche UC process and mechanism of erbium-doped ZBLAN glass at room temperature [22–24]. But its unique properties are not only limited to the application of luminescence, but also aroused interest in different fields. For example, a recent study found that through continuous wave pumping, the emission intensity of the $^3F_4$ intermediate state energy level of Tm^{3+} ions non-linearly expands to the 26th power with the pumping intensity, and the application of super-resolution imaging has been realized. This also provides research ideas for the detection of the COVID-19 virus that has recently swept the world [1]. In the PA material doped with lanthanides, a single GSA triggers a chain reaction between the ESA and Ln^{3+} ions in the cross-relaxation process, which will result in a large number of photon emission [1].

The crystal field around the dopant ion has a great influence on the UC efficiency. Compared with high symmetry crystals, low symmetry crystals will generate more asymmetric crystal fields around the dopant ions, thereby greatly improving the UC efficiency. For example, the $NaBi(WO_4)_2$(NBW) crystal, which has been studied more in recent years, has a non-centrosymmetric tetragonal crystal structure space group $\bar{I}41/a$ $\bar{I}41/a$ [24], therefore, a more asymmetric crystal field will be generated around the rare earth ions, which increases the probability of the 4f-4f transition of the rare earth ions, and the NBW crystal has a disordered structure, which is due to the irregular distribution of Bi^{3+} and Na^+ ions in the crystal lattice, which leads to an increase in emission intensity [25–27]. However, in order to achieve the expected photon avalanche phosphor, it is very important to select the appropriate RE ions. Since Ho^{3+} ions have intermediate sub-energy levels and stable $^5I_5$ and $^5I_6$ energy levels, these characteristics greatly promote the efficiency of excited state absorption and cross-relaxation processes [28].

Therefore, in this article, we report Yb^{3+} and Ho^{3+} co-doped NBW phosphors, and found that the cross-relaxation and energy cycling process of Ho^{3+} ions produce extreme nonlinear PA phenomenon. By obtaining the average of the number of photons and the rise time of the green light emission level with power, the photon absorption process was observed and verified, and the PA process was explained by the cycle mechanism.

2 Materials and characterization

A series of Yb^{3+}/Ho^{3+} co-doped $NaBi(WO_4)_2$ phosphors were synthesized by hydrothermal method. High-purity sodium tungstate ($Na_2WO_4 \cdot 2H_2O$) (99.5%), holmium Oxide (Ho_2O_3) (99.99%), ytterbium oxide (Yb_2O_3) (99.99%), bismuth nitrate ($Bi(NO_3)_3 \cdot 5H_2O$) (99.9%) are used as starting materials. Before the reaction starts, the rare earth oxide is first dissolved in concentrated nitric acid to form nitrate (RE $(NO_3)_3$), and a certain amount of $Na_2WO_4 \cdot 2H_2O$ is uniformly dissolved in 20 mL of deionized water. The amount of each chemical calculated according to the ingredients, nitrates RE(NO_3)$_3$, and $Bi(NO_3)_3 \cdot 5H_2O$ are dissolved in 20mL of deionized water. Then slowly add the sodium tungstate solution to the nitric acid solution to form a suspension, and keep the mixed solution under acidic conditions and stir for 30 min, transfer it to a stainless steel autoclave (70

mL). In the experiment, the reaction kettle was kept at 220 ☐ for 18 h. After standing, it was naturally cooled to room temperature, and the reaction product was centrifuged. washed with deionized water and absolute ethanol 3 times, and then dried in air at 60 ☐ for 20 h to obtain the final sample.

Use CuK-α radiation source (k=0.1546 nm, 40 kV, 20 mA) X-ray powder diffractometer (XRD-7000, SHIMADZU) in the range of 10°–80°, 5°/min scan rate to characterize the test sample. Scanning electron microscopy (SEM, EVOMA-25, ZEISS) was used for morphological studies. The absorption spectrum was measured by Perkin Elmer Co., Ltd. (Lambda 950 UV-VIS). A spectrophotometer (FLS920, Edinburgh Instruments) was used to measure the up-conversion emission spectra and fluorescence decay curves of the red and green emission under 980 nm excitation.

3 Results and discussion

3.1 Yb^{3+}, Ho^{3+}: $NaBi(WO_4)_2$ structure and morphology analysis

The XRD of the NBW phosphor doped with different concentrations of Yb^{3+} ions are depicted in Fig. 1a. All diffraction peaks are consistent with the diffraction peaks of standard card (JCPDS#52-1718), and no miscellaneous peaks are detected, indicating that the NBW: $1\%Ho^{3+}$, $x\%Yb^{3+}$ compound has been successfully prepared, and the substitution of Yb^{3+}, Ho^{3+} ions have no significant effect on the crystal structure. In addition, as shown in Fig. 1b, as the Yb^{3+} ion concentration increases, the diffraction

peaks regularly shift to large angles. This is because Bi^{3+} has a larger radius and is larger than rare earth ions (Ho^{3+}: 0.0901 nm, Yb^{3+}: 0.0868 nm, Bi^{3+}:0.096- nm). According to the Bragg equation $2d\sin\theta = n\lambda$, when Bi^{3+} ions are replaced by Yb^{3+} and Ho^{3+} ions with a smaller ion radius, the lattice constant and the distance between planes (d) decrease, the diffraction angle increases. As a result, the main diffraction peak is shifted to large angle.

Figure 2a is the absorption spectrum of NBW phosphors, there are absorption peaks located at 451, 488, 528, and 655 nm, which are attributed to the $^5I_8$ to $^5G_6$, $^5F_2+^5F_3$, $^5F_4+^5S_2$, and $^5F_5$ energy of Ho^{3+} ions, respectively [29, 30]. The optical band gap of NBW: $1\%Ho^{3+}$, $x\%Yb^{3+}$ phosphor was calculated by Wood and Tauc formula [31], as shown below:

$$\alpha = \frac{B(hv - E_g)^m}{hv}$$

where E_g is the optical band gap, hv is the incident photon energy, and B is the band adjustment constant. For transitions that are directly allowed, the value of the constant "m" is taken as $1/2$. Figure 2b shows the curve drawn between $(\alpha hv)^2$ and hv for Ho^{3+} and Yb^{3+} co-doped NBW phosphors, with a direct optical band gap of 2.97 eV. As shown in Fig. 2c, d the optical band gap of NBW gradually decreases with the doping of rare earth ions. As we all know, one of the main factors affecting the luminous intensity is the microscopic morphology of the sample. Regular and uniform size is the most ideal microscopic morphology, and the sample exhibits high cumulative density, which can reduce light

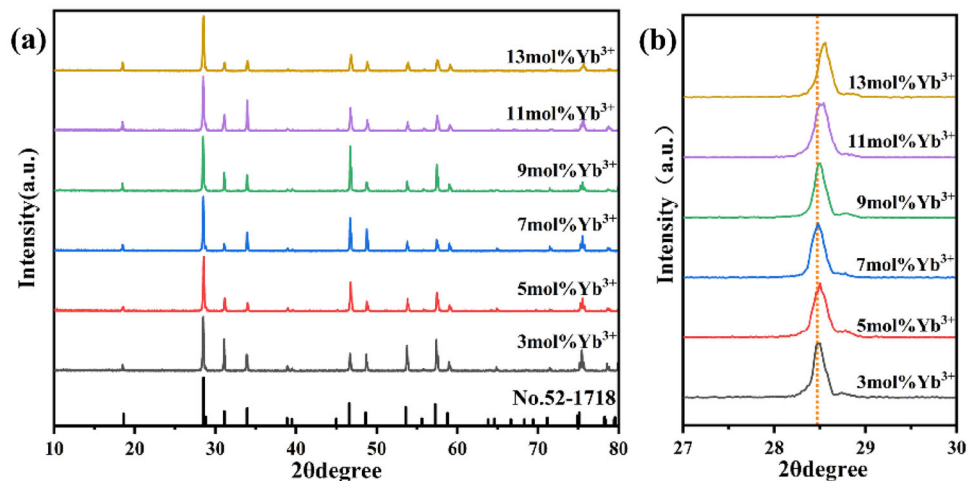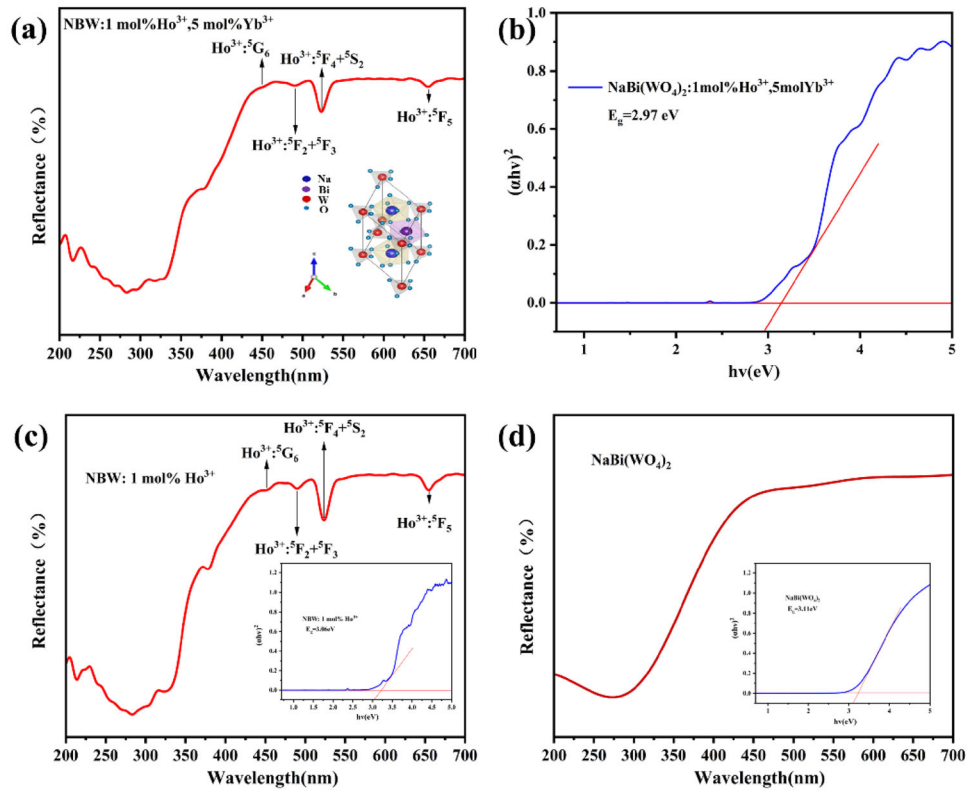Fig. 1 a XRD patterns of NBW: $1\%Ho^{3+}$, $x\%Yb^{3+}$ and the main peak patterns b of NBW: $1\%Ho^{3+}$, $x\%Yb^{3+}$

Fig. 2 Absorption spectrum of sample **a** NBW: 1%Ho^{3+}, 5%Yb^{3+}, **c** NBW: 1%Ho^{3+} and **d** NaBi(WO$_4$)$_2$. **b** the $(\alpha h\nu)^2 \sim h\nu$ curves of sample NBW: 1%Ho^{3+}, 5%Yb^{3+}

scattering in addition to obtaining high luminous efficiency. SEM images of representative samples NBW: 1%Ho^{3+}, 5%Yb^{3+} are shown in Fig. 3a, b. Obviously, the samples observed under SEM are in sheet-like and multi-faceted morphology, which indicates that the crystallinity of the particles is very high. The element composition and uniformity of NBW: Yb, Ho were determined by EDS. The average atomic ratio Na/Bi/W is 0.06: 2.57: 15.52, which is close to the formula NaBi(WO$_4$)$_2$, and the element mapping image Fig. 3c–j also indicates the uniform distribution of elements in the phosphor particles.

3.2 Research on up-conversion of Yb, Ho: NaBi(WO$_4$)$_2$ phosphor

Figure 4 shows the UC emission spectrum and R/G emission intensity ratio of NBW: 1%Ho^{3+}, x%Yb^{3+} measured at room temperature. The $^5S_2/^5F_4 \rightarrow {}^5I_8$ of Ho^{3+} ion produces green emission at 541 nm, while the $^5S_2/^5F_4 \rightarrow {}^5I_8$ transition produces red emission at 644 nm [32, 33]. Both red and green emission gradually increase with the increase of Yb^{3+} ion concentration (3 mol%→11 mol%) and the luminous intensity reaches the peak at 11 mol% Yb^{3+}, and then there is concentration quenching, resulting in the

luminous intensity at 13 mol% Yb^{3+} reduce. In order to understand the enhancement of red and green emission in depth, The energy level diagram in Fig. 5 shows the energy transfer process of Yb$^{3+} \rightarrow$ Ho^{3+} ions.

The energy transfer mechanism between Yb^{3+} and Ho^{3+} ions is described in detail in Fig. 5. In this work, Yb^{3+} ion is selected as the sensitizer, so we only consider the two energy levels of Yb^{3+}, so its absorption cross section is very large. When Yb^{3+} ion absorbs 980 nm laser, it is excited from $^2F_{7/2}$ state to $^2F_{5/2}$ state, it can effectively transfer energy to Ho^{3+} ions. This makes it easy for the large amount of energy absorbed by Yb^{3+} ions to be transferred to Ho^{3+} ions [34]. In low concentration Yb^{3+} ion doping, the pump energy absorbed by Yb^{3+} ion passes ET1 $[^2F_{5/2}(Yb^{3+})+{}^5I_8(Ho^{3+})\rightarrow{}^2F_{7/2}(Yb^{3+})+{}^5I_6(Ho^{3+})$, ET2 $[^2F_{5/2}(Yb^{3+})+{}^5I_6(Ho^{3+})\rightarrow{}^2F_{7/2}(Yb^{3+})+{}^5S_2/^5F_4(Ho^{3+})]$, ET3$[^2F_{5/2}(Yb^{3+})+{}^5I7(Ho^{3+})\rightarrow{}^2F_{7/2}(Yb^{3+})+{}^5F_5(Ho^{3+})]$ can fill the $^5S_2/^5F_4$ and $^5F_5$ energy levels, respectively, producing green and red emission [35, 36]. According to the analysis of Yb and Ho energy transfer in the figure above, the UC emission at 541 and 644 nm
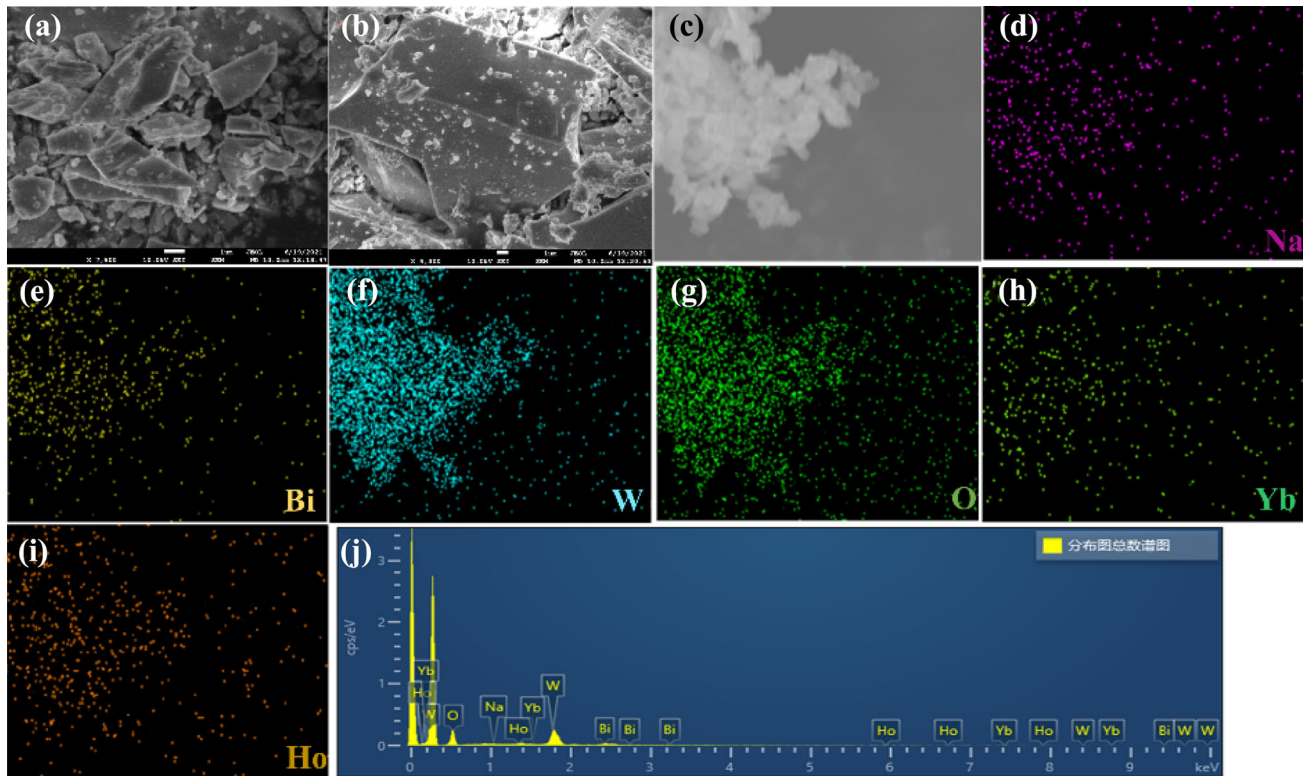
Fig. 3 SEM image of NBW: 1%Ho^{3+}, 5%Yb^{3+} phosphor (**a**) and **b** under high magnification, and EDS element mapping image (**c**–**j**)
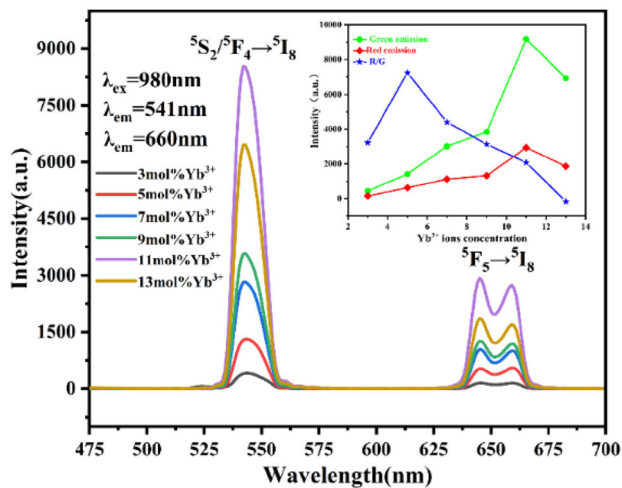
Fig. 4 UC spectra of NBW: 1%Ho^{3+}, x%Yb^{3+} phosphors excited at 980 nm of light at room temperature

Fig. 5 Energy transfer process (simplified) of Ho^{3+} and Yb^{3+} ions in the NBW matrix under excitation at 980 nm

occurs through a two-photon process. However, due to the PA process, our results show that the average number of photons emitted by UC is greater than 5.

3.2.1 Avalanche mechanism

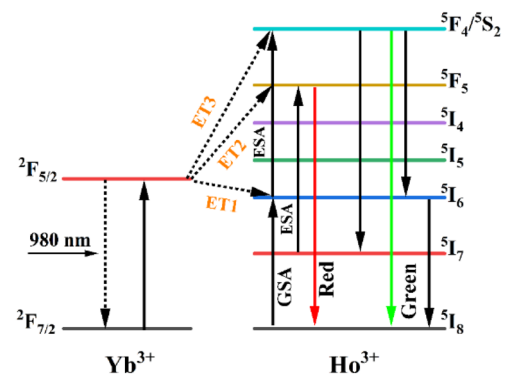According to reports, the conventional PA mechanism has two notable features: The first typical

feature is the non-linear increase of the slope n of UC emission under the pump power threshold. This can be explained by the "s"-shaped power dependence. The increase is usually caused by positive feedback filling the intermediate energy level [37, 38]. The observation in Fig. 6 is similar to this situation. The second is to use square wave excitation technology to perform instantaneous pacing measurement, where the conventional PA mechanism shows a sudden non-linear upward trend at the pump power

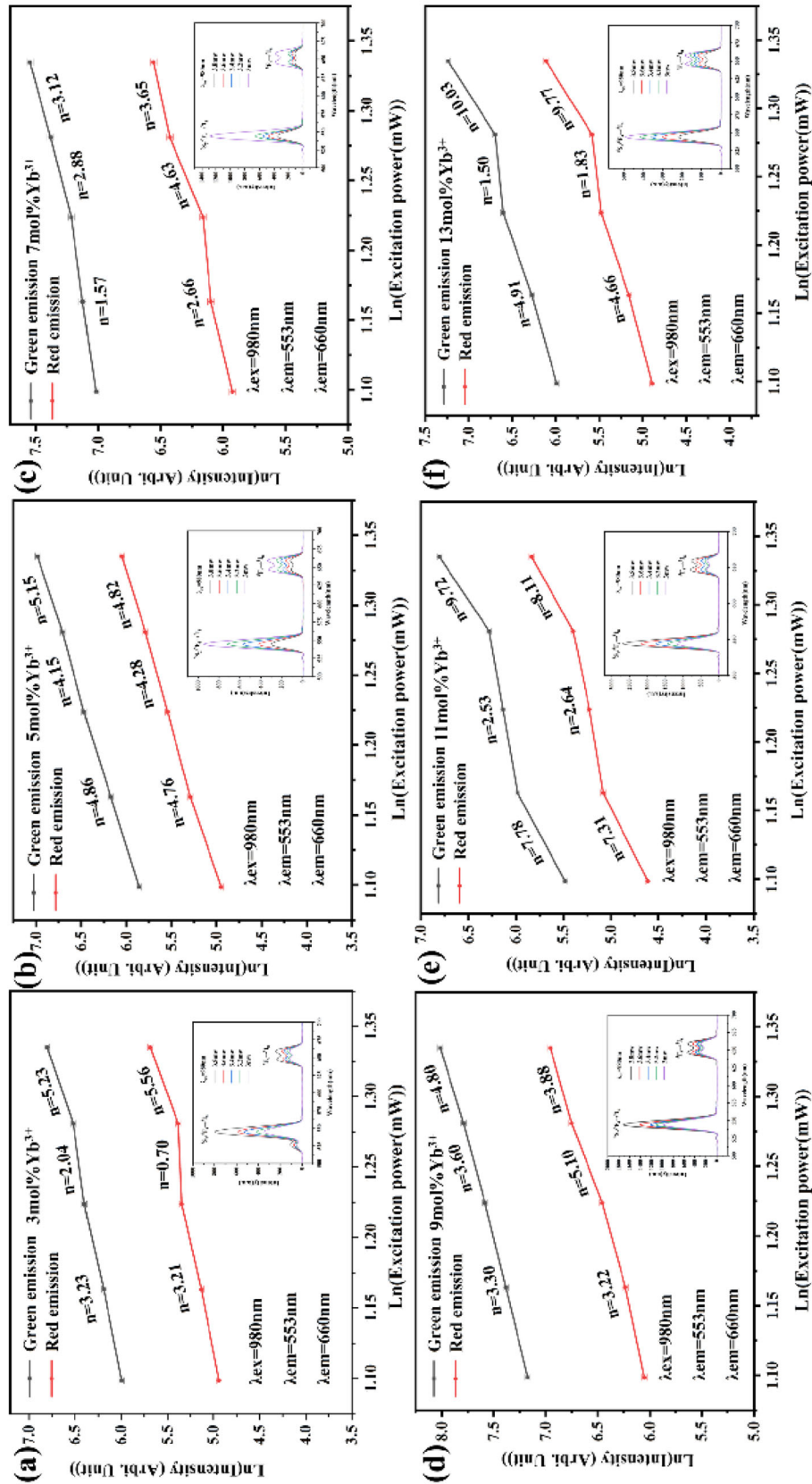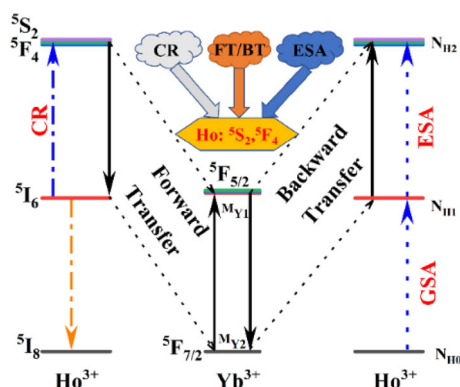**Fig. 6** Power dependence of the green and red emission (553, 660 nm) of NBW: 1%Ho^{3+}, x%Yb^{3+} phosphors under 980 nm laser excitation

Fig. 7 Simplified three level model for looping process CR, GSA, ESA, FT, and BT($Ho^{3+} \rightarrow Yb^{3+} \rightarrow Ho^{3+}$)

threshold, while in continuous two-photon absorption only a linear upward trend is displayed.

In this effect, pumping corresponds to the absorption of intermediate excited state energy levels (metastable state), rather than the common pure electron absorption from ground state to excited state. Generally speaking, this method of pumping is impossible, but the intermediate energy level starts to be filled through the PA process, and then the pump light is strongly absorbed. Two necessary conditions must be met to construct this process: (1) Excited state absorption (ESA) is produced by a long-lived intermediate energy level [39]; (2) The intermediate energy level is filled by some effective cross-relaxation processes [40]. Therefore, this puts special requirements on the doped ions and concentration, and the host material. In addition to the disparity in the pumping scheme, there are also differences in other aspects between the ordinary up-conversion and the PA process. Generally speaking, the nonlinear dependence and threshold value of the PA process on the pump power have a much longer stabilization time than the normal UC luminescence process, and the stabilization time is related to the pump intensity.

In Fig. 6, we find the nonlinear behavior between the UC emission intensity and laser power, and this mutation phenomenon is only found in the visible light emission band. This means that not only the excited state absorption, but also the existence of a cyclic process, instead of the traditional PA process. Recently, Shivkumar et al. proposed the Hetrolooping Enhanced Energy Transfer (H-LEET) process to explain this process. H-LEET process energy transfer

up-conversion and positive feedback/cyclic process and non-zero ground state absorption. The biggest difference between the PA process and the H-LEET process is the non-zero ground state absorption. But the nonlinear power dependence of the H-LEET and PA processes is similar [37, 41]. Goldner et al. discussed the theoretical limitations of the PA process and proposed a cross-relaxation enhanced excited state absorption (CRESA) mechanism [42]. However, CRESA is based on the inherently less efficient GSA/ESA process. Only described in terms of single crystal.

In order to describe the energy transfer method in the PA process in more detail, we have omitted other irrelevant energy levels, so the simplified model of the cyclic process is shown in Fig. 7. We use the following up-conversion and cycling process to explain the PA process found in NBW. First, 980 nm photons fill the $^5I_6$ energy level through GSA. Through three different processes, $^5I_6$ energy level ions are further promoted to $^5S_2$:$^5F_4$ energy level; through energy transfer processes, CR and ESA energy transfer processes (Fig. 7). In Ho^{3+}, a few energy transitions are very similar, namely $^5I_8 \rightarrow ^5I_7$ and $^5S_2 \rightarrow ^5I_4$ (resonance), $^5I_4 \rightarrow ^5I_6$ and $^5I_7 \rightarrow ^5I_6$ (non-resonance), $^5S_2 \rightarrow ^5I_6$ and $^5I_8 \rightarrow ^5I_6$ (resonance), these transfer processes make cross. The relaxation process fills the $^5S_2$ energy level, resulting in an avalanche effect [9].

In the presence of Yb^{3+} ions, energy passes forward energy transfer (FT) [$Ho^{3+} \rightarrow Yb^{3+}$;($^5S_2$:$^5F_4$, $^2F_{7/2}$) $\rightarrow$($^5I_6$, $^2F_{5/2}$)] and reverse energy transfer (BT) [$Yb^{3+} \rightarrow Ho^{3+}$; ($^2F_{5/2}$,$^5I_8$)$\rightarrow$($^2F_{7/2}$,$^5I_6$)] proceed [9], Therefore, the energy transfer and CR process compete with each other, forming two cycles, namely Ho^{3+}-Ho^{3+} cycles caused by cross-relaxation between ions and FT/BT cycles (Fig. 7). The excited state at the $^5I_6$ energy level. The two Ho^{3+} ions are produced by the Ho^{3+} ions at the $^5S_2$:$^5F_4$ energy level from two cycles, and they can also be used to absorb incident pump light. This is a process of multiplication, and four excited Ho^{3+} ions are generated during the next cycle. Therefore, the PA process took place.

In this work, the PA process is based on the CR, FT, and BT processes that lead to an increase in the number of photons in the $^5I_6$ and $^5S_2$:$^5F_4$ energy levels [35], therefore, we use the theoretical rate equation model to evolve the total energy and its changes over time [43]:

For Ho^{3+} ion:

$$\frac{dN_0}{dt} = -R_{GSA}N_0 - r_{CR}N_2N_1 - r_{BT}M_1N_0$$
$$+ (A_2 + A_{20})N_1 + B_{20}A_2N_2$$

$$\frac{dN_1}{dt} = -(A_1 + A_{10})N_1 - R_{ESA}N_1 + R_{GSA}N_0$$
$$+ (1 - B_{20})A_2N_2 + A_{20}N_2 + 2r_{CR}N_2N_0$$
$$+ r_{FT}M_0N_2 + r_{FT}M_1N_0$$

$$\frac{dN_2}{dt} = -(A_2 + A_{20})N_2 - r_{CR}N_2N_0 - r_{FT}M_0N_2$$
$$+ R_{ESA}N_1$$

$$N_0 + N_1 + N_2 = 1$$

For Yb^{3+} ion:

$$\frac{dM_0}{dt} = -r_{FT}M_0N_2 + A_{M_{11}}M_1 + r_{BT}M_1N_0$$

$$\frac{dM_1}{dt} = -A_{M1}M_1 + r_{FT}M_1N_2 - r_{BT}M_1N_0$$

$$M_1 + M_2 = 1$$

Among them, R_{ESA} and R_{GSA} are the pumping rates of the excited state and ground state, respectively; M_i and N_i are the population in ith level of Yb^{3+} and Ho^{3+} ions; r_{FT} is the forward transfer efficiency [$(N_2,M_0) \rightarrow (N_1,M_1)$]; R_{CR} is the CR rate of the entire process;, r_{BT} is the reverse transfer efficiency [$(M_1, N_0) \rightarrow (M_0, N_1)$], B_{ji} is branch ratio of $j \rightarrow i$; A_i, A_{i0} are the radiative and non-radiative transition rates of the energy level [44, 45].

We calculated the cross-relaxation, forward and reverse energy transfer rates, and analyzed the cyclic process between Yb^{3+} and Ho^{3+} ions in depth (Table 1).

The non-radiative relaxation process dominates only when the ion concentration is high, so the life value calculated by the exponential function fitting has a large error. In this case, only the effective relaxation rate and average lifetime can be calculated. We calculated the effective lifetime of the $^2F_{5/2}$ energy level of Yb^{3+} ion and the $^5S_2$, $^5F_4$ energy level of Ho^{3+} ion using the following relationship:

$$\tau^{eff} = \frac{\int_0^\infty I(t)dt}{I(0)dt}$$

where $I(t)$ represent the emission intensity at time t after the incident beam is completely cut off. As the concentration of Ho^{3+} increases, the lifetime of red and green emission decreases significantly due to the cross-relaxation process. Figure 8 shows the decay curves of $^5S_2$ and $^5F_4$ levels. The CR rate W_{CR} can be calculated by the following relationship [46]:
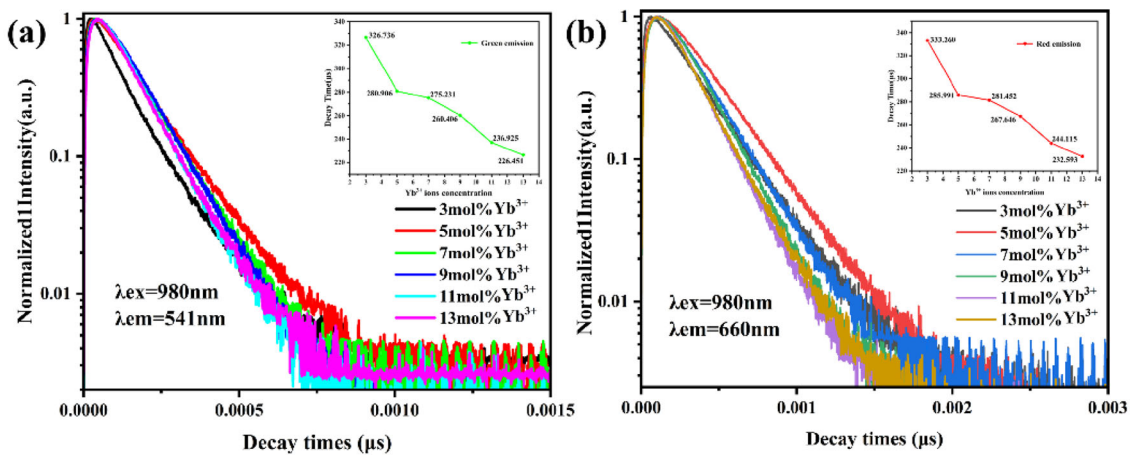
Table 1 Effective decay time (μs) and cross-relaxation rate (W_{CR}) of Ho^{3+} ion ($^5S_2$, $^5F_4$ level)

Concentration(mol%)				
Ho^{3+}	Yb^{3+}	τ ($^5S_2,^5F_4$)	τ ($^5F_{5/2}$)	W_{CR}
1	3	326.736	336.260	–
1	5	280.906	285.991	49
1	7	275.231	281.452	73
1	9	260.406	267.646	206
1	11	236.925	244.115	380
1	13	226.451	232.593	195

Fig. 8 Decay profile of NBW: 1%Ho^{3+}, x%Yb^{3+} with different concentration of Yb^{3+} ions at room temperature

$$W_{CR} = \frac{1}{\tau^{eff}\{^5S_2, ^5F_4\}(x)} - \frac{1}{\tau^{eff}\{^5S_2, ^5F_4\}(0.1mol\%)}$$

where x is the concentration of Yb^{3+} ions. When the CR rate is from 3→5 mol%, there is 49 S^{-1}. When it increases to 11 mol%, there is 380 S^{-1}. Therefore, under the condition of ytterbium ion co-doping, the energy transfer process occurs between Ho^{3+}→ Yb^{3+}→Ho^{3+} ions.

4 Conclusion

Under the excitation of 980 nm laser, the abnormal "s"-shaped pump power dependence of UC emission in NBW: Yb, Ho phosphor was observed. It was found that the $^5S_2/^5F_4$→$^5I_8$ of Ho^{3+} ion produces green emission at 541 nm, while the $^5S_2/^5F_4$→$^5I_8$ transition produces red emission at 644 nm. Both red and green emission gradually increase with the increase of Yb^{3+} ion concentration (3 mol%→11 mol %) and the luminous intensity reaches the peak at 11 mol% Yb^{3+}, and then there is concentration quenching, and the cross-relaxation and energy cycling process of Ho^{3+} ions produced an extreme nonlinear photon avalanche. By obtaining the average of the number of photons and the rise time of the green light emission level with power, the photon absorption process was observed and verified. The cyclic mechanism explains the PA process, that is, the CR, FT, BT process causes the number of photons at the $^5I_6$ and $^5S_2/^5F_4$ energy levels to double. At the same time, the theoretical results analyzed by the rate equation model are consistent with the experimental results. These results have important application value in the detection material of temperature sensor plays an important role, it also provides unprecedented opportunities for technological innovation.

Acknowledgments

Author contributions

HQ: conceptualization, data curation, formal analysis, writing—original draft. TZ: data curation, software, formal analysis, writing—editing. XJ: formal analysis, writing—review. HW: formal analysis, methodology. WY: investigation, methodology. CL: Conceptualization, supervision, funding acquisition, resources, supervision.

Data availability

The data that support the findings of this study are available from the corresponding author upon reasonable request.

Declarations

Conflict of interest The authors declare that they have no known competing financial interests or personal relationships that could have appeared to influence the work reported in this paper.

References

1. C. Lee, E. Xu, Y.W. Liu, A. Teitelboim, K.Y. Yao, A. Fernandez-Bravo, A. Kotulska, S.H. Nam, Y.D. Suh, A. Bednarkiewicz, B.E. Cohen, E.M. Chan, PJ. Schuck. Nature. **589**, 230–235 (2021)
2. S.K. Singh, K. Kumar, S.B. Rai, Sens. Actuat A-Phys **149**, 16–20 (2009)
3. R. Dey, V.K. Rai, Dalton T. **43**, 111–118 (2014)
4. F. Wang, Y. Han, C.S. Lim, Y.H. Lu, J. Wang, J. Xu, H.Y. Chen, C. Zhang, M.H. Hong, XG. Liu. Nature. **463**, 1061–1065 (2010)
5. Y. Dwivedi, S.B. Rai, J. Am. Ceram. Soc. **93**, 727–731 (2010)
6. E. Downing, L. Hesselink, J. Ralston, R. Macfarlane. Science. **273**, 1185–1189 (1996)
7. P. Zhang, W. Steelant, M. Kumar, M. Scholfield, J. Am. Ceram. Soc. **129**, 4526–4527 (2007)
8. AS. E.B. Gouveia-Neto, L.A. Costa, Bueno, SJL. Ribeiro. Journal Alloy Compd. 375, 224–228 (2004)
9. Y. Dwivedi, A. Bahadur, S.B. Rai, J. Appl. Phys. **110**, 043103 (2011)
10. A. Kumar, A. Bahadur, J. Alloy Compd **857**, 158196 (2020)

11. M.F. Joubert, Opt. Mater. **11**, 181–203 (1999)

12. A. Bednarkiewicz, E. Chan, A. Kotulska, L. Marciniak, K. Prorok. Nanoscale Horiz. **4**, 881–889 (2019)

13. M.A. Mahdia, S.R. Yousefi, L.S. Jasima, M. Salavati-Niasari, Int. J. Hydrogen Energ. **47**, 14319–14330 (2022)

14. S.R. Yousefi, H.A. Alshamsi, O. Amiri, M. Salavati-Niasari, J. Mol. Liq **337**, 116405 (2021)

15. S.R. Yousefi, D. Ghanbari, M. Salavati-Niasari, M. Hassanpour, J. Mater. Sci-Mater El **27**, 1244–1253 (2015)

16. S.R. Yousefi, M. Ghanbari, O. Amiri, Z. Marzhoseyni, P. Mehdizadeh, M. Hajizadeh-Oghaz, M. Salavati-Niasari, J. Am. Ceram. Soc. **104**, 2952–2965 (2021)

17. S.R. Yousefi, A. Sobhani, H.A. Alshamsic, M. Salavati-Niasari, RSC Adv. **11**, 11500–11512 (2021)

18. S.R. Yousefi, O. Amiri, M. Salavati-Niasari, Ultrason. Sonochem **58**, 104619 (2019)

19. S.R. Yousefi, M. Masjedi-Arani, M.S. Morassaei, M. Salavati-Niasari, Int. J. Hydrogen Energ. **44**, 24005–24016 (2019)

20. M. Salavati-Niasari, A. Sobhani, S.R. Yousefi, J. Soc. Powder Technol. Japan **28**, 1258–1262 (2017)

21. S.R. Yousefi, D. Ghanbari, Masoud Salavati Niasari. J Nanostruct **27**(2), 1244–1253 (2017)

22. H. Deng, S.H. Yang, S. Xiao, H.M. Gong, Q.Q. Wang, J. Am. Ceram. Soc. **130**, 2032–2040 (2008)

23. F. Lahoz, I.R. Martín, V.L. Guadalupe, J. Mendez-Ramos, V.D. Rodriguez, UR. Rodriguez-Mendoza. Opt Mater. **25**, 209–213 (2004)

24. F. Auzel, Y.H. Chen, D. Meichenin, J. Lumin. **60**, 692–694 (1994)

25. J.H. Xie, L.Q. Chen, H. Tang, X.F. Yu, C.B. Wang, X.Y. Mi, Q.S. Liu, XY. Zhang. J Lumin. **219**, 116841 (2019)

26. M.H. Li, L.L. Wang, W.G. Ran, Z.H. Deng, C.Y. Ren, JS. Shi. Ceram Int. **43**, 6751–6757 (2017)

27. C.L. Ma, H. Cui, F.F. Li, J. Wang, X.X. Wu, J. Zhang, Q. Zhou, J.H. Liu, QL. Cui. J Solid State Chem **200**, 246–250 (2013)

28. T.Q. Zhang, W.L. Yang, H.B. Li, X.Y. Wang, X.L. Jiang, Z. Leng, W.L. Yang, C. Li, H. Lin, H.S. Liu, K.K. Huang, C. Li, F.M. Zeng, ZM. Su. J Lumin. **240**, 118432 (2021)

29. A.M. Pires, MR. Davolos. Chem Mater. **13**, 21–27 (2001)

30. T. Jiang, Y. Tian, M.M. Xing, Y. Fu, X.M. Yin, H. Wang. Mater Res Bull **98**, 328–334 (2018)

31. X.L. Jiang, X.Y. Wang, X.M. Shi, H.Y. Sha, W.J. Yang, W.L. Yang, Z. Leng, H. Lin, Z.M. Su, C. Li, F.M. Zeng, Opt. Mater. **113**, 110873 (2021)

32. X.C. Yu, Y.B. Qin, M.L. Gao, L. Duan, Z.Q. Jiang, L. Gou, P. Zhou, Z. Li, J. Lumin. **153**, 1–4 (2014)

33. Z.F. Shan, D.Q. Chen, Y.L. Yu, P. Huang, F.Y. Weng, H. Lin, YS. Wang. Mater Res Bull. **45**, 1017–1020 (2010)

34. M.M. Xing, W.H. Cao, H.Y. Zhong, Y.H. Zhang, X.X. Luo, F. Yao, W. Feng, T. Pang, X.F. Yang, J. Alloy Compd. **509**, 5725–5730 (2011)

35. X.J. Tan, S.L. Xu, F.H. Liu, X.Y. Wang, B.A. Goodman, D.K. Xiong, W. Deng. J Lumin **209**, 95–101 (2019)

36. J.F. Tang, C.H. Cheng, Y.J. Chen, YD. Huang. J Alloy Compd. **609**, 268–273 (2014)

37. G.Y. Chen, H.J. Liang, H.C. Liu, G. Somesfalean, Z.G. Zhang, J. Appl. Phys. **105**, 114315 (2009)

38. R. Scheps, Prog Quant. Electron. **20**, 271–358 (1996)

39. A. Franois, Chem. Rev. **104**, 139–173 (2004)

40. E.S. Levy, C.A. Tajon, T.S. Bischof, J. Iafrati, A. Fernandez-Bravo, DJ. Garfield. Acs Nano. **10**, 8423–8433 (2016)

41. S. Sivakumar, V. Veggel, P. May, J. Am. Ceram. Soc. **129**, 620–625 (2007)

42. P. Goldner, F. Pelle, Opt. Mater. **5**, 239–249 (1996)

43. E. Osiac, I. Sokólska, S. Kück, Phy Rev. B **65**, 235119 (2002)

44. E. Osiac, I. Sokólska, S. Kück. J Lumin. **94**, 289–292 (2001)

45. X.F. Wang, S.G. Xiao, Y.Y. Bu, X.L. Yang, JW. Ding. Opt Lett. **33**, 2653–2655 (2008)

46. A.I. Burshtein, J. Lumin. **34**, 167–188 (1985)